Morphology of Three Lyotropic Liquid Crystalline Biological NMR Media Studied by Translational Diffusion Anisotropy

Sander Gaemers and Ad Bax*

Contribution from the Laboratory of Chemical Physics, National Institute of Diabetes and Digestive and Kidney Diseases, National Institutes of Health, Bethesda, Maryland 20892-0520

Received August 13, 2001

Abstract: The morphologies of three dilute liquid crystalline phases, which are widely used for biological NMR spectroscopy, are investigated by the study of tracer self-diffusion. The aqueous liquid crystalline media investigated include the common phospholipid bicelle medium, a phase consisting of a mixture of pentaethyleneglycol mono dodecyl ether and hexanol, and a medium containing cetylpyridinium bromide and hexanol. Threonine and water were used as tracer molecules for probing the aqueous environment, and tetramethylsilane (TMS) was for probing the lipophilic environment. Pulsed field gradient NMR was used to measure tracer self-diffusion rates in three orthogonal directions. Although results for the water-soluble tracers in bicelle media do not contradict the widely accepted disk-shaped bicelle model, the high TMS diffusion rate observed in the bilayer plane requires extensive transient edge-to-edge contacts of such disks. This morphology is essentially that of a heavily perforated lamellar bilayer phase and explains why this medium remains liquid crystalline well below the Onsager limit for disk-shaped nematogens. Below 25 °C, a bicelle mixture consisting of dimyristoyl phosphatidyl choline and dihexanoyl phosphatidyl choline remains isotropic, but tracer diffusion obstruction indicates that the particles are significantly oblate. The diffusion anisotropy in the penta(ethyleneglycol) mono dodecyl ether liquid crystals confirms the previously proposed α-lamellar phase. However, weak inhibition of aqueous-phase self-diffusion in the *z* direction points to the presence of bridge- or caplike obstructions, and the bilayers appear slightly permeable to water. If the previously proposed concentric cylinder superstructure of bilayers applies, the diffusion data indicate that the most outer cylinder must have a diameter greater than 50 μm. The tracer self-diffusion data for the cetylpyridinium bromide/hexanol medium is only compatible with a planar α-lamellar phase, with its local director orthogonal to the magnetic field, and a very large domain size over which the director remains parallel.

Introduction

Weak alignment of a macromolecule with an external magnetic field either can occur as a result of its magnetic susceptibility anisotropy[1,2] or may be induced by the use of a weakly anisotropic medium.[3] Provided the degree of solute alignment is sufficiently weak (typically $<10^{-3}$), only the largest dipolar interactions yield observable effects in the NMR spectrum, which then retains the simplicity of the regular isotropic high-resolution NMR spectrum. These dipolar couplings have proven invaluable for improving the accuracy of macromolecular NMR structure determination,[4,5] for independently validating this accuracy,[6−9] for refining crude homology models of proteins,[10] and for defining intermolecular interactions.[11,12] Dipolar couplings also offer the possibility to search for homologous structures or substructures in a structure database[13,14] and potentially could replace the time-consuming regular NOE data collection and analysis process.[15,16] Most dipolar couplings used so far are of the one-bond type, although the utility of ^{1}H−^{1}H interactions has also been established.[17−19]

Alignment induced by a molecule's magnetic susceptibility anisotropy frequently is insufficient for measuring the residual dipolar couplings at the required degree of accuracy. When using a dilute aqueous liquid crystalline phase, the degree of order

* To whom correspondence should be addressed at: Building 5, Room 126, NIH, Bethesda, MD 20892-0520. Fax: 301 402 0907. E-mail: bax@nih.gov.

(1) Bothner-By, A. A. In *Encyclopedia of Nuclear Magnetic Resonance*; Grant, D. M., Harris, R. K., Ed.; Wiley: Chichester, U.K., 1996; Vol. 5, pp 2932−2938.
(2) Tolman, J. R.; Flanagan, J. M.; Kennedy, M. A.; Prestegard, J. H. *Proc. Natl. Acad. Sci. U.S.A.* **1995**, *92*, 9279−9283.
(3) Tjandra, N.; Bax, A. *Science* **1997**, *278*, 1111−1114.
(4) Tjandra, N.; Omichinski, J. G.; Gronenborn, A. M.; Clore, G. M.; Bax, A. *Nat. Struct. Biol.* **1997**, *4*, 732−738.
(5) Bewley, C. A.; Gustafson, K. R.; Boyd, M. R.; Covell, D. G.; Bax, A.; Clore, G. M.; Gronenborn, A. M. *Nat. Struct. Biol.* **1998**, *5*, 571−578.
(6) Cornilescu, G.; Marquardt, J. L.; Ottiger, M.; Bax, A. *J. Am. Chem. Soc.* **1998**, *120*, 6836−6837.
(7) Clore, G. M.; Garrett, D. S. *J. Am. Chem. Soc.* **1999**, *121*, 9008−9012.
(8) Drohat, A. C.; Tjandra, N.; Baldisseri, D. M.; Weber, D. J. *Protein Sci.* **1999**, *8*, 800−809.
(9) Ottiger, M.; Bax, A. *J. Biomol. NMR* **1999**, *13*, 187−191.
(10) Chou, J. J.; Li, S.; Bax, A. *J. Biomol. NMR* **2000**, *18*, 217−227.
(11) Olejniczak, E. T.; Meadows, R. P.; Wang, H.; Cai, M. L.; Nettesheim, D. G.; Fesik, S. W. *J. Am. Chem. Soc.* **1999**, *121*, 9249−9250.
(12) Clore, G. M. *Proc. Natl. Acad. Sci. U.S.A.* **2000**, *97*, 9021−9025.
(13) Annila, A.; Aitio, H.; Thulin, E.; Drakenberg, T. *J. Biomol. NMR* **1999**, *14*, 223−230.
(14) Meiler, J.; Peti, W.; Griesinger, C. *J. Biomol. NMR* **2000**, *17*, 283−294.
(15) Delaglio, F.; Kontaxis, G.; Bax, A. *J. Am. Chem. Soc.* **2000**, *122*, 2142−2143.
(16) Hus, J. C.; Marion, D.; Blackledge, M. *J. Mol. Biol.* **2000**, *298*, 927−936.
(17) Tjandra, N.; Marquardt, J.; Clore, G. M. *J. Magn. Reson.* **2000**, *142*, 393−396.
(18) Tjandra, N.; Tate, S.; Ono, A.; Kainosho, M.; Bax, A. *J. Am. Chem. Soc.* **2000**, *122*, 6190−6200.
(19) Martin-Pastor, M.; Bush, C. A. *J. Biomol. NMR* **2001**, *19*, 125−139.

10.1021/ja011967l
Published on Web 11/16/2001

induced on the solute macromolecule depends linearly on the surface area of the liquid crystal. This makes it possible to tune the degree of solute alignment by adjusting the volume fraction of liquid crystal in water.[20−22]

The first such liquid crystalline phase used for this purpose is the phospholipid bicelle medium.[3] Bicelles are commonly described as disk-shaped phospholipid bilayers, with the edges of these disks covered by detergent,[23−25] but this monodisperse disk model has been questioned.[26] After bicelles, a range of other liquid crystalline media has been demonstrated to achieve the desired weak degree of macromolecular alignment. These include rodlike virus particles (phages),[22,27] cetylpyridinium-halide/*n*-hexanol mixtures,[28,29] cellulose particles,[30] and *n*-alkyl-poly(ethyleneglycol)/*n*-hexanol (PEG/*n*-hexanol).[31] Purple membrane fragments have sufficiently large individual magnetic susceptibility anisotropy to align with the strong fields used in biological NMR and can be used as an alignment medium without requiring a liquid crystalline phase.[32,33] Another recent and potentially very useful alignment method uses strained hydrogels containing anisotropic cavities.[34,35] The alignment of water-soluble biomolecules in the above media results from the combined effect of steric and electrostatic interactions.[36]

The morphology and phase behavior of many dilute liquid crystals tends to be sensitive to parameters such as temperature, ionic strength, concentration, pH, and the addition of ionic and nonionic cosurfactants.[37] Although detailed phase diagrams and scattering studies are available for many binary and ternary water/surfactant systems,[38] only a few of these solutions have a liquid crystalline phase with a composition and temperature range suitable for biomolecular NMR. Knowledge of the morphology of lyotropic liquid crystals is essential to improve our quantitative understanding of the biomolecular alignment in such media. The present paper studies this morphology for three different liquid crystalline phases for which the literature models have been questioned. These include dilute liquid crystalline phases of bicelles, cetylpyridinium bromide/*n*-hexanol (CPBr), and PEG/*n*-hexanol mixtures. Our study relies on the measurement of diffusion anisotropy of tracer molecules present in the liquid crystalline solution.[39−45] This method not only provides information on short-range structure but also is an invaluable tool for the study of macroscopic order in these media.

The most common bicelle medium consists of a mixture of the long-chain phospholipid 1,2-di-tetradecanoyl-*sn*-glycero-3-phosphocholine (DMPC) and the detergent 1,2-di-hexanoyl-*sn*-glycero-3-phosphocholine (DHPC), but a range of slightly different long-chain phospholipids and detergents has also been used to extend the temperature and pH range over which the liquid crystalline phase remains stable.[9,21,46−49] In the disk-shaped bicelle model, the detergent surrounds the disk in a hemitoroidal manner and shields the hydrophobic DMPC alkyl chains from solvent. The phospholipid:detergent ratio is believed to control the size of the disks.[25] The virtual absence of NOE contacts between DMPC and DHPC under conditions where the sample adopts liquid crystalline order confirms their partitioning to separate regions.[50,51] Small amounts of charged amphiphiles such as cetyltrimethylammonium bromide (CTAB) or sodium dodecyl sulfate (SDS) can be adsorbed in the bicelles and can improve the stability of the nematic liquid crystalline phase, presumably through repellant electrostatic interaction.[47,52] The bicelle medium was originally developed to study lipophilic molecules, anchored in the bilayer, by solid-state NMR,[24,53,54] and the medium was then used at quite high volume fractions (20−30%). For NMR studies of macromolecules in the aqueous phase, typically very low volume fractions are used (3−10%).[20,21] Importantly, rotational diffusion rates of molecules in the aqueous fraction of the liquid crystalline medium are not affected by the bicelles,[20] but transverse translational diffusion is strongly impeded and, together with translational diffusion of molecules adsorbed in the bilayers, provides information on morphology.

Prosser et al.[28] proposed the use of a cetylpyridinium chloride (CPCl)/hexanol/salt mixture as a liquid crystalline matrix for weakly orienting solute macromolecules. This mixture forms an α-lamellar phase that is stabilized by electrostatic repulsion and entropic effects [55,56] Barrientos et al.[29] proposed the use of cetylpyridinium bromide (CPBr), which reportedly permits the use of low ionic strengths. The morphology of this CPBr

(20) Bax, A.; Tjandra, N. *J. Biomol. NMR* **1997**, *10*, 289−292.
(21) Ottiger, M.; Bax, A. *J. Biomol. NMR* **1998**, *12*, 361−372.
(22) Hansen, M. R.; Mueller, L.; Pardi, A. *Nat. Struct. Biol.* **1998**, *5*, 1065−1074.
(23) Sanders, C. R.; Schwonek, J. P. *Biochemistry* **1992**, *31*, 8898−8905.
(24) Sanders, C. R.; Hare, B. J.; Howard, K. P.; Prestegard, J. H. *Prog. Nucl. Magn. Reson. Spectrosc.* **1994**, *26*, 421−444.
(25) Vold, R. R.; Prosser, R. S. *J. Magn. Reson., Ser. B* **1996**, *113*, 267−271.
(26) Sanders, C. R.; Prosser, R. S. *Struct. Fold. Des.* **1998**, *6*, 1227−1234.
(27) Clore, G. M.; Starich, M. R.; Gronenborn, A. M. *J. Am. Chem. Soc.* **1998**, *120*, 10571−10572.
(28) Prosser, R. S.; Losonczi, J. A.; Shiyanovskaya, I. V. *J. Am. Chem. Soc.* **1998**, *120*, 11010−11011.
(29) Barrientos, L. G.; Dolan, C.; Gronenborn, A. M. *J. Biomol. NMR* **2000**, *16*, 329−337.
(30) Fleming, K.; Gray, D.; Prasannan, S.; Matthews, S. *J. Am. Chem. Soc.* **2000**, *122*, 5224−5225.
(31) Ruckert, M.; Otting, G. *J. Am. Chem. Soc.* **2000**, *122*, 7793−7797.
(32) Koenig, B. W.; Hu, J. S.; Ottiger, M.; Bose, S.; Hendler, R. W.; Bax, A. *J. Am. Chem. Soc.* **1999**, *121*, 1385−1386.
(33) Sass, J.; Cordier, F.; Hoffmann, A.; Cousin, A.; Omichinski, J. G.; Lowen, H.; Grzesiek, S. *J. Am. Chem. Soc.* **1999**, *121*, 2047−2055.
(34) Tycko, R.; Blanco, F. J.; Ishii, Y. *J. Am. Chem. Soc.* **2000**, *122*, 9340−9341.
(35) Sass, H. J.; Musco, G.; Stahl, S. J.; Wingfield, P. T.; Grzesiek, S. *J. Biomol. NMR* **2000**, *18*, 303−309.
(36) Zweckstetter, M.; Bax, A. *J. Am. Chem. Soc.* **2000**, *122*, 3791−3792.
(37) Hoffmann, H. *Ber. Bunsen-Ges. Phys. Chem.* **1994**, *98*, 1433−1455.
(38) Chernik, G. G. *Curr. Opin. Colloid Interface Sci.* **1999**, *4*, 381−390.
(39) Tanner, J. E.; Stejskal, E. O. *J. Chem. Phys.* **1968**, *49*, 1768−1777.
(40) Callaghan, P. T.; Soderman, O. *J. Phys. Chem.* **1983**, *87*, 1737−1744.
(41) Johannesson, H.; Furo, I.; Halle, B. *Phys. Rev. E* **1996**, *53*, 4904−4917.
(42) Coppola, L.; Muzzalupo, R.; Ranieri, G. A.; Terenzi, M. *Langmuir* **1995**, *11*, 1116−1121.
(43) Lindblom, G.; Oradd, G. *Prog. Nucl. Magn. Reson. Spectrosc.* **1994**, *26*, 483−515.
(44) Jonsson, B.; Wennerstrom, H.; Nilsson, P. G.; Linse, P. *Colloid Polym. Sci.* **1986**, *264*, 77−88.
(45) Chung, J.; Prestegard, J. H. *J. Phys. Chem.* **1993**, *97*, 9837−9843.
(46) Sanders, C. R.; Prestegard, J. H. *Biophys. J.* **1990**, *58*, 447−460.
(47) Sanders, C. R.; Landis, G. C. *Biochemistry* **1995**, *34*, 4030−4040.
(48) Wang, H.; Eberstadt, M.; Olejniczak, E. T.; Meadows, R. P.; Fesik, S. W. *J. Biomol. NMR* **1998**, *12*, 443−446.
(49) Cavagnero, S.; Dyson, H. J.; Wright, P. E. *J. Biomol. NMR* **1999**, *13*, 387−391.
(50) Sternin, E.; Nizza, D.; Gawrisch, K. *Langmuir* **2001**, *17*, 2610−2616.
(51) Luchette, P. A.; Vetman, T. N.; Prosser, R. S.; Hancock, R. E. W.; Nieh, M. P.; Glinka, C. J.; Krueger, S.; Katsaras, J. *Biochim. Biophys. Acta-Biomembr.* **2001**, *1513*, 83−94.
(52) Losonczi, J. A.; Prestegard, J. H. *J. Biomol. NMR* **1998**, *12*, 447−451.
(53) Sanders, C. R.; Landis, G. C. *J. Am. Chem. Soc.* **1994**, *116*, 6470−6471.
(54) Howard, K. P.; Prestegard, J. H. *J. Am. Chem. Soc.* **1995**, *117*, 5031−5040.
(55) Helfrich, W. *Z. Naturforsch.* **1978**, *C33*, 305−315.
(56) McGrath, K. M. *Langmuir* **1997**, *13*, 1987−1995.

medium is still a matter of debate, and evidence for formation of long flexible cylinders at increasing salt concentrations has been presented,[57,58] and the possibility of a rodlike liquid crystal matrix has been raised. In another recent NMR study, the system is described as being a lamellar phase with its symmetry axis parallel to the magnetic field.[59]

The PEG/*n*-hexanol based liquid crystal has a number of features that make it particularly attractive for biomolecular NMR. The liquid crystalline medium is found to be quite robust and easy to make by mixing commercially available materials. The liquid crystal can simply be removed by dialysis, and ethylene-glycol is noncharged and known to generally have low affinity for biological macromolecules. PEG is believed to form lamellar structures that orient with the normal of the plane perpendicular to the magnetic field and have a superstructure of sets of concentric cylinders,[31,60] similar to structures observed in freeze fracture transmission electron micrographs of ternary tetradecyldimethylaminoxide/*n*-heptanol/water mixtures.[37] However, the dilute conditions used for NMR are close to the transition to a sponge-type phase in the PEG phase diagram,[61,62] and the precise morphology therefore is still unclear.

The present study measures the translational diffusion rates of three different tracer molecules in the above liquid crystalline phases in order to characterize their morphology. Water and threonine diffusion rates are used to report on the aqueous fraction of the suspensions, whereas tetramethylsilane (TMS) partitions in the hydrophobic bilayers and complements the aqueous phase data.

Experimental Section

Materials. DMPC and DHPC (Avanti Polar Lipids), $C_{12}E_5$ (≥ 98% purity, Fluka), *n*-hexanol (98% purity, Aldrich), TMS (99.9%, Aldrich), cetylpyridinium bromide monohydrate (98%, Aldrich), NaBr (99.99+%, Aldrich), L-threonine (*allo* free, A-grade, Calbiochem), D_2O (99.9%, Cambridge Isotope Laboratories), and NaOD in D_2O solution 40% (w/w) (Cambridge Isotope Laboratories) were all used as received.

NMR Sample Preparation. The dilute liquid crystal solutions were prepared according to literature procedures.[21,29,31] All samples were prepared in D_2O containing 15 mM phosphate buffer (pH = 7.54); threonine was added, after which the pH was adjusted using a NaOD in D_2O solution. Finally, after TMS was added, the samples were vortexed and transferred to NMR sample tubes. The final concentration of the volatile TMS was determined from the ratio of the integrated ^{1}H NMR intensities of the methyl groups in threonine and TMS.

Bicelle samples were prepared at 5% (w/v) and 10% (w/v), q = [DMPC]/[DHPC] = 3.2, pH = 7.2, 39 mM threonine, 3.8 mM TMS. Two bicelle samples were prepared at 10% (w/v) lipids, one without addition of CTAB and one with the addition of CTAB in a 1:20 molar ratio relative to DMPC. Comparison of the integrated ^{31}P resonance intensities for the liquid crystalline bicelle samples confirmed the accuracy of their relative concentrations. At the low concentrations used, addition of TMS to the bicelle samples was found to be nonperturbing as judged by identical solvent ^{2}H quadrupole splittings, ^{31}P spectra, and temperature ranges over which the sample remains liquid crystalline. However, at [TMS]/[DMPC] ≥ 0.1, TMS clearly perturbs the liquid crystalline ordering, and TMS concentrations well below this threshold were therefore used throughout.

The $C_{12}E_5$ sample contained 8 wt % liquid crystal ($C_{12}E_5$) plus *n*-hexanol at a molar ratio of [$C_{12}E_5$]/[*n*-hexanol] = 0.93, pH = 7.34, 25 mM threonine, 4.1 mM TMS. The CPBr sample contained 6% (w/v) liquid crystal (CPBr + *n*-hexanol) at a relative weight fraction CPBr/*n*-hexanol (w/w) = 1/1.35, pH = 6.88, 5 mM NaBr, 23 mM threonine, 5.2 mM TMS. A small amount of excess hexanol, floating on top of the liquid crystalline phase after equilibration of the sample, was removed with a pipet.[29] A sample containing 39 mM threonine in 15 mM phosphate buffer was used as an isotropic reference sample and will be further referred to as the isotropic D_2O solution.

To restrict the sample volume to the region over which the field gradients are most linear, all experiments were carried out in Shigemi microcells (Shigemi Inc., Allison Park, PA), with the sample length carefully adjusted to 14 mm for all samples. To avoid the formation of air bubbles, the samples were spun in the Shigemi microcells at 120 g for ∼5 min at room temperature before adjusting the plunger to its final position in the sample tube and sealing the tube with Parafilm. Our standard procedure of degassing Shigemi NMR samples by exposing the unsealed tube to a low pressure (ca. 50 mbar) could not be used, as the added TMS evaporates at reduced pressures (bp 26−28 °C).

NMR Experiments. All spectra were recorded on a Bruker DMX-600 NMR spectrometer operating at a ^{1}H frequency of 600 MHz and containing a triple resonance probehead with self-shielded pulsed field gradients in the *x*, *y*, and *z* directions. The liquid crystalline nature of the samples was confirmed by observing the quadrupolar splitting of the deuterium signal of the D_2O. Deuterium spectra were recorded before and after the self-diffusion experiments and did not change over the course of the experiments.

Diffusion experiments in bicelles were carried out at temperatures ranging from 10 to 35 °C. Measurements in CPBr and $C_{12}E_5$ media were carried out at 25 °C, but the $C_{12}E_5$ liquid crystal sample was briefly heated to 40 °C, above its liquid crystal to isotropic phase transition temperature, prior to diffusion measurements at 25 °C. This heating cycle was found to increase the homogeneity and long-term stability of the observed D_2O quadrupole splitting, leaving it constant to within ±4% over a 24 h period.

The pulsed field gradient (PFG) NMR experiment used here is a modified version of the standard longitudinal encode−decode sequence[63,64] and includes an element for suppression of convection artifacts.[65] After completion of all measurements, several of the rates were remeasured with the standard sequence, yielding identical results within the random measurement error, indicating that convection does not play a role in the high-viscosity samples used in our study. The pulsed field gradients were calibrated on the residual ^{1}H signal in a sample of 99.9% D_2O, using the recommended value of $1.902 \pm 0.002 \times 10^{-9}$ m^2 s^{-1} for the self-diffusion coefficient of HDO at 25 °C.[66−69] The sample-averaged gradient strengths were found to be 49.1, 50.4, and 66.8 G/cm at the maximum current for the *x*, *y*, and *z* gradient coils, respectively, with no discernible deviation from linearity relative to programmed values over the entire gradient amplitude range. Square gradients of increasing strength, from 2.5 to 65% of the maximum current, were used and a duration of 3 ms each. For each sample, two decay curves in each of the *x*, *y*, and *z* directions were measured using diffusion delays (Δ) of 150 and 600 ms.

Fitting of Diffusion Decay Data. Decay curves of the diffusion experiments were fit to the various models using the software package Mathematica. For cases where the signal decay is visibly nonexponential, reported rates are the initial decay rates, obtained from fits of data points that correspond to the first 40% of the decay.

Theoretical Section

This study aims to determine the morphology of various liquid crystalline media by analysis of the translational diffusion

(57) Porte, G.; Appell, J.; Poggl, Y. *J. Phys. Chem.* **1980**, *84*, 3105−3110.
(58) Porte, G.; Gomati, R.; Elhaitamy, O.; Appell, J.; Marignan, J. *J. Phys. Chem.* **1986**, *90*, 5746−5751.
(59) Reddy, V. B.; Fung, B. M. *Langmuir* **2001**, *17*, 3563−3566.
(60) Burnell, E. E.; Capitani, D.; Casieri, C.; Segre, A. L. *J. Phys. Chem. B* **2000**, *104*, 8782−8791.
(61) Strey, R.; Glatter, O.; Schubert, K. V.; Kaler, E. W. *J. Chem. Phys.* **1996**, *105*, 1175−1188.
(62) Freyssingeas, E.; Nallet, F.; Roux, D. *Langmuir* **1996**, *12*, 6028−6035.
(63) Gibbs, S. J.; Johnson, C. S. *J. Magn. Reson.* **1991**, *93*, 395−402.
(64) Altieri, A. S.; Hinton, D. P.; Byrd, R. A. *J. Am. Chem. Soc.* **1995**, *117*, 7566−7567.
(65) Jerschow, A.; Muller, N. *J. Magn. Reson.* **1997**, *125*, 372−375.
(66) Mills, R. *J. Phys. Chem.* **1973**, *77*, 685−688.
(67) Holz, M.; Weingartner, H. *J. Magn. Reson.* **1991**, *92*, 115−125.
(68) Price, W. S. *Concepts Magn. Reson.* **1997**, *9*, 299−336.
(69) Price, W. S. *Concepts Magn. Reson.* **1998**, *10*, 197−237.

anisotropy of tracer molecules dissolved in these media. The obstruction inhibition of translational diffusion in ordered liquid crystals is highly anisotropic and is a function of the shape and orientation of the liquid crystal particles. PFG-NMR is a proven tool for studying the morphology of liquid crystals.[40,41,43,68] However, none of these previous studies dealt with the dilute liquid crystals investigated here. Various models have been derived which describe the apparent self-diffusion in lamellar and capillary environments. In the case of uninhibited diffusion the signal intensity decay is a function of the encoding and decoding gradient duration, δ, the gradient strength, g, and the diffusion delay Δ between the encoding and decoding gradients:[68,70]

$$I(g,\delta,\Delta) = I_0 e^{(-kD)} \tag{1}$$

where, in the short gradient pulse limit, $k = (\gamma_H \delta g)^2 \Delta$, with γ_H the gyromagnetic ratio of ^{1}H, D the translational self-diffusion coefficient, I_0 the signal intensity at zero gradient, and $I(g,\delta,\Delta)$ the signal intensity as a function of g, δ, and Δ. Each of these parameters may be varied in a PFG-NMR diffusion experiment to obtain the desired diffusion-dependent signal intensity modulation. In practice, only g is altered in a series of small steps, which minimizes errors introduced by relaxation during the gradient pulses and the diffusion delay.

For diffusion in a lamellar environment, $D_{||}$ and $D_\perp$ are the self-diffusion coefficients in the directions parallel and perpendicular to the normal of the bilayer plane, respectively. For diffusion in a direction that makes an angle θ with the bilayer normal, the diffusion constant equals

$$D(\theta) = D_\perp \sin^2\theta + D_{||} \cos^2\theta \tag{2a}$$

In the magnetically ordered systems considered in this paper, the bilayer normal is orthogonal to the magnetic field. If, on average, this bilayer normal does not have a preferred direction (i.e., bilayers do not remain parallel across the entire sample), the signal decay resulting from diffusion in a direction orthogonal to the magnetic field is given by

$$I(g,\delta,\Delta) = \frac{2}{\pi}\int_0^{\frac{\pi}{2}} e^{-D(\theta)k}\,d\theta = \frac{2}{\pi}\int_0^{\frac{\pi}{2}} e^{-[D_\perp \sin^2\theta + D_{||}(1-\sin^2\theta)]k}\,d\theta \tag{2b}$$

$$= \frac{2}{\pi} e^{-D_{||}k}\int_0^{\frac{\pi}{2}} e^{-[(D_\perp - D_{||})\sin^2\theta]k}\,d\theta$$

So, the observed signal intensity is given by

$$I(g,\delta,\Delta) = I_0 e^{-D_{||}k}\int_0^{\frac{\pi}{2}} e^{-[(D_\perp - D_{||})\sin^2\theta]k}\,d\theta \tag{2c}$$

where the factor $2/\pi$ has been absorbed in I_0.

In general, $D_{||}$ and $D_\perp$ are quite different, and therefore the decay of eq 2c is nonexponential. However, if the orientation of the bilayer normal is random in the transverse plane on the length scale over which the tracer molecule diffuses during the delay between the encoding and decoding gradients, i.e., ca. $\sqrt{(2D_\perp\Delta)}$, averaging of $D_{||}$ and $D_\perp$ takes place, resulting in exponential decay:

$$I(g,\delta,\Delta) = I_0 e^{-(D_{||}+D_\perp)k/2} \tag{2d}$$

Diffusion in the direction parallel to the magnetic field occurs at a rate $D_\perp$, and when using z gradients the signal decay is simply described by

$$I(g,\delta,\Delta) = I_0 e^{-D_\perp k} \tag{2e}$$

For the case of a perfectly ordered lamellar phase, with infinitely large lamellar planes, the value of $D_\perp$ for a water soluble tracer will approach that of its isotropic diffusion constant.

In a system consisting of homogeneously distributed, anisotropic impenetrable objects, the self-diffusion coefficient of a tracer molecule will be reduced compared to a system without obstructions. The obstruction is commonly expressed as the ratio of a principal component of the macroscopic diffusion tensor with and without obstruction,

$$A_{\alpha\alpha} = D_{\alpha\alpha}/D_0 \tag{3}$$

where $D_{\alpha\alpha}$ is the self-diffusion coefficient in a medium containing obstructions (with $\alpha = x, y, z$) and D_0 is the isotropic self-diffusion coefficient in the absence of obstruction. The obstruction factor has been described in ordered macrofluids[71] and colloidal systems[44] and is related to the particle shape and its concentration.

The obstruction factor may be calculated using either the effective medium approximation (EMA)[72] or the effective cell approximation (ECA).[43] The EMA model describes a system with obstructions of a given shape, taking the surrounding obstructions into account in an average way. In the case of the ECA model, the obstruction is replaced by an effective cell of the same size as the true obstruction, adding a solvation shell to account for the volume fraction of the system. Numerical calculations indicate that at low obstruction volume fractions (<25%, as applies in the present study) the ECA model is best suited for predicting the obstruction factors $A_{||}$ and $A_\perp$.[71] The obstruction factors for diffusion parallel ($A_{||}$) and perpendicular ($A_\perp$) to the unique axis of oblate spheroid obstructions, as described by the ECA model, are given by[44,71]

$$A_{||} = \frac{1}{1-\Phi}\left[1 - \frac{\Phi}{1 - h(\xi_s) + \Phi h(\xi_c)}\right] \tag{5a}$$

$$A_\perp = \frac{1}{1-\Phi}\left[1 - \frac{2\Phi}{1 + h(\xi_s) + \Phi[1 - h(\xi_c)]}\right] \tag{5b}$$

with

$$h(\xi) = (\xi^2 + 1)[1 - \xi\,\mathrm{arccot}(\xi)] \tag{5c}$$

and the ξ_c and ξ_s values determined by the aspect ratio (r) and volume fraction (Φ) of the obstructions:

$$\xi_s = \frac{1}{\sqrt{\rho^2 - 1}} \tag{5d}$$

$$\xi_c(\xi_c^{\,2} + 1) = \frac{1}{\Phi}\xi_s(\xi_s^{\,2} + 1) \tag{5e}$$

Results and Discussion

For molecules diffusing in an axially symmetric liquid crystalline medium, both $D_{||}$ and $D_\perp$ are experimentally accessible. The bilayered liquid crystals used in this study align with their bilayer normal perpendicular to the magnetic field. Therefore, diffusion in the direction of the magnetic field ($D_\perp$) will be little affected by the presence of the obstructions,

(70) Stejskal, E. O.; Tanner, J. E. *J. Chem. Phys.* **1965**, *42*, 288−292.
(71) Johannesson, H.; Halle, B. *J. Chem. Phys.* **1996**, *104*, 6807−6817.
(72) Fricke, H. *Phys. Rev.* **1924**, *24*, 575−587.

whereas diffusion in a direction orthogonal to the magnetic field ($D_{||}$) is affected much stronger.

All NMR experiments were carried out in D_2O solution, allowing the residual ^1H signal of HDO to be used as a tracer molecule and circumventing the need for suppression of the H_2O signal and problems associated with radiation damping. Threonine was added as a second tracer molecule to the D_2O solutions in order to probe the aqueous part of the dilute liquid crystals and to identify potential problems related to slower water diffusion in the first hydration shell of the bilayer. Owing to its hydrophilic amino and carboxyl groups, threonine cannot traverse the bilayers and shuttle exchangeable water protons across. However, even if threonine, PEG, or hexanol were able to do this, their concentration relative to that of the ca. 100 M water hydrogens is too low for causing a significant effect. TMS was used as a tracer molecule to probe the interior of the apolar bilayers of the liquid crystals. As mentioned in the Experimental Section, at the low concentrations used, TMS has no measurable effect on the phase diagram or aligning properties of any of the three liquid crystals studied.

For each of the liquid crystals the self-diffusion coefficients of HDO, threonine, and TMS were determined in the *x*, *y*, and *z* directions. The obstruction factors (eq 3) for HDO and threonine in the liquid crystalline media were determined by comparison with the corresponding self-diffusion coefficients in isotropic D_2O solution. In all diffusion experiments the gradient pulse width (3 ms) and interpulse duration (600 ms) are held constant, and the signal intensity is modulated only by the strength of the pulsed field gradient. Therefore, below we simply refer to this intensity as $I(g)$. Data derived from a second set of diffusion decay curves, recorded at 150 ms interpulse duration, are provided as Supporting Information.

Isotropic Bicelles. The self-diffusion coefficients of HDO, threonine, and TMS were determined in three different bicelle solutions, containing 5 and 10% (w/v) lipids, in the absence of the charged amphiphile CTAB, and also at 10% (w/v) in the presence of CTAB. At 20 °C the samples are isotropic and the self-diffusion coefficients along the *x*, *y*, and *z* axes are indistinguishable. Signal decay as a function of gradient strength is exponential (Supporting Information Figure 1). The experimental self-diffusion coefficients and obstruction factors are reported in Table 1.

TMS is insoluble in water and partitions almost exclusively in the bicelles. The TMS diffusion rate therefore provides an upper limit for the diffusion rate of the phospholipid particle. The translational self-diffusion rate of a particle, with a volume equivalent to that of a sphere with radius *R* (the effective radius), is given by

$$D = \frac{k_B T}{6\pi\eta RF} \tag{6}$$

where k_B is the Boltzmann constant, *T* is the absolute temperature, *F* is the Perrin shape factor which is larger than one for nonspherical particles, and η is the solvent viscosity.[73] The TMS diffusion rate at a 5% bicelle concentration and 20 °C yields an effective radius of ca. 70 Å for the phospholipid particle. Considering that the length of the fatty acid DMPC chains is only about 14 Å, a spherical phospholipid particle is not realistic and presumably the bicelle is disk shaped below the DMPC melting temperature of 25 °C. If the particle is assumed to be an oblate spheroid, with a thickness of 40 Å, eq 6 yields a diameter of about 200 Å. However, the TMS diffusion rate increases slightly when lowering the temperature (data not shown), despite the increase in water viscosity. Moreover, the diffusion rate is also a function of the charge of the phospholipid particle, as evidenced by the effect of adding CTAB (Table 1). This suggests that introduction of repellant electrostatic interaction between the particles increases their rate of diffusion. Both observations argue against the inert, hard-sphere particle model required for validity of eq 6. The effective particle size at low temperature therefore cannot accurately be determined from the TMS data reported in Table 1. Transient interaction between the phospholipid particles is supported by a steep increase in the macroscopic viscosity of the bicelle phospholipid solution, by up to several orders of magnitude, when the temperature approaches the melting temperature of the DMPC alkyl chains.[74]

Table 1. Self-Diffusion Coefficients and Obstruction Factors of HOD, Thr, and TMS in Isotropic Bicelles at 20 °C

		bicelle concentration[a]		
		5%	10%	10% + CTAB[b]
HDO	$D_{\alpha\alpha}$[c]	15.5 ± 0.1	14.6 ± 0.1	15.2 ± 0.1
	$A_{\alpha\alpha}$[d]	0.93 ± 0.01	0.87 ± 0.01	0.91 ± 0.01
Thr	$D_{\alpha\alpha}$[c]	5.14 ± 0.05	4.74 ± 0.03	5.00 ± 0.05
	$A_{\alpha\alpha}$[d]	0.93 ± 0.01	0.86 ± 0.01	0.90 ± 0.01
TMS	$D_{\alpha\alpha}$[c]	0.25 ± 0.01	0.14 ± 0.01	0.26 ± 0.01

[a] Bicelle concentrations are in w/v, with q = [DMPC]/[DHPC] = 3.2. [b] Bicelles included CTAB in a molar ratio [DMPC]/[CTAB] = 20. [c] Self-diffusion coefficients in units of 10^{-10} m^2 s^{-1}. Uncertainties in the self-diffusion coefficients, $D_{\alpha\alpha}$ ($\alpha = x, y, z$), are determined from the spread in D_{xx}, D_{yy}, and D_{zz}, and the uncertainty in the fitted slopes. [d] Obstruction factors ($A_{zz} = D_{zz}/D_0$) calculated using isotropic diffusion coefficients (D_0) of 16.7 × 10^{-10} m^2 s^{-1} for HDO and 5.55 × 10^{-10} m^2 s^{-1} for threonine.

The obstruction factor of water-soluble tracer molecules is an additional parameter providing insight into the shape and size of particles present in colloidal suspensions. An upper bound for the average obstruction factor in a macroscopically homogeneous and isotropic system is given by[71]

$$\langle A \rangle \leq \frac{1}{1 + \Phi/2} \tag{7}$$

where Φ is the volume fraction of the colloid particles. Equation 7 applies for spherical particles and yields $\langle A \rangle = 0.95$ for a 10% (w/v) suspension (using a density of 1.04 g/mL for the phospholipids). The HDO obstruction factors observed in the 10% (w/v) isotropic bicelle solutions are 0.87 ± 0.01 and 0.91 ± 0.01 in the absence and presence of CTAB (Table 1). Using the ECA model (eq 5), and for simplicity assuming oblate spheroidal shapes, these obstruction factors correspond to aspect ratios, ρ, of 7 ± 1 and 5 ± 1 in the absence and presence of CTAB. Assuming a thickness of 40 Å, this yields particle diameters of 280 ± 40 and 200 ± 40 Å in the absence and presence of CTAB, respectively. Clearly, these numbers are only very approximate because, as argued above, the assumption of noninteracting, fixed shape particles is not valid. Nevertheless, these data indicate a smaller and less oblate particle size in the presence of CTAB, in agreement with the above-noted faster diffusion rates observed for the signal of TMS, encapsulated in the lipid particles. The low values observed for $\langle A \rangle$ also exclude prolate or wormlike morphologies, for which a much higher value of $\langle A \rangle$ is predicted.[71]

Liquid Crystalline Bicelles. The DMPC/DHPC bicelle suspension forms a nematic liquid crystalline phase over the range from 27 to 44 °C, but in the absence of charged

(73) Cantor, C. R.; Schimmel, P. R. *Biophysical Chemistry*; Freeman: San Francisco, 1980; Vol. Part 2.

(74) Struppe, J.; Vold, R. R. *J. Magn. Reson.* **1998**, *135*, 541−546.

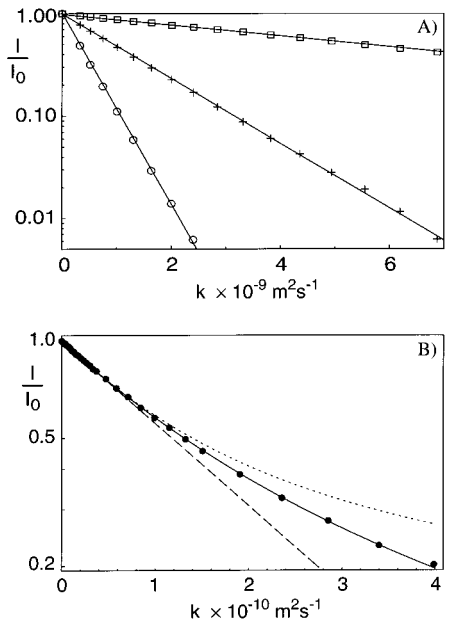

Figure 1. Tracer signal decay as a function of gradient strength in liquid crystalline bicelles at 35 °C, using a 600 ms diffusion delay. (A) Signal decay for HDO (O), threonine (+), and TMS (□) when using *z* gradients. (B) TMS signal decay when applying *x* gradients. Long dashes correspond to exponential decay, with the rate derived from a best fit of the initial decay. Short dashes correspond to the lamellar model with $D_{||} = 0$ and $D_{\perp} = 1.1 \times 10^{-10}$ m^2 s^{-1}. The solid line corresponds to the lamellar model with $D_{||} = 0.116 \times 10^{-10}$ m^2 s^{-1} and $D_{\perp} = 1.1 \times 10^{-10}$ m^2 s^{-1}.

amphiphiles it can turn unstable near the lower end of this temperature range.[21,52] At 35 °C the order imposed by the bicelles on the solvent resulted in stable ^{2}H quadrupolar splittings of 7.2 and 16.6 Hz for the 5 and 10% (w/v) samples in the absence of CTAB and 18.4 Hz for the 10% CTAB-bicelle sample. The slightly higher ^{2}H splitting for the CTAB-containing sample appears largely due to a higher degree of order for the bicelles and is also reflected in a 0.5 ppm upfield shift of the DMPC ^{31}P resonance, which as a result of its chemical shielding anisotropy is shifted upfield of its isotropic value.[21,23]

For all three tracer molecules, signal decay resulting from self-diffusion in the *z* direction is exponential (Figure 1A). However, for TMS, signal decay resulting from transverse self-diffusion is highly nonexponential (Figure 1B). Such multi-exponential behavior is expected when the tracer is confined to a bilayer with its normal randomly oriented in the transverse plane (cf. eq 2c). The self-diffusion rates derived from these data are summarized in Table 2. For TMS, the transverse self-diffusion rate is derived from the initial slope at low gradient strengths. Also included in this table are the obstruction factors, obtained from eq 3 and the isotropic diffusion coefficients reported in the footnote to Table 1.

The initial slope of the TMS diffusion decay curve indicates an approximately 2-fold slower $D_{x,y}$ than D_{zz}. For a perfectly ordered planar structure, with its norm orthogonal to the magnetic field, $D_{zz} = D_{\perp}$, and $D_{x,y} = (D_{||} + D_{\perp})/2$. Therefore, the data reported in Table 2 indicate that $D_{||} \approx 0$, i.e., that diffusion of TMS in a direction parallel to the bilayer normal is extremely slow. In contrast, TMS diffusion in the *z* direction occurs at an appreciable rate, which far exceeds the rate of self-diffusion expected for a model bicelle disk of 400 Å diameter and 40 Å thickness. This therefore suggests that TMS can exchange between bicelles. The absence of interbicelle TMS exchange in the direction of the bilayer normal, which would result in nonzero $D_{||}$, suggests that the exchange occurs through (transient) fusion of the bicelles in an edge-on manner.

Table 2. Self-Diffusion Coefficients and Obstruction Factors in Liquid Crystalline Bicelle Suspensions at 35 °C

		bicelle concentration[a]		
		5%	10%	10% + CTAB[b]
HDO	D_{zz}[c]	23.4 ± 0.3	21.7 ± 0.2	22.7 ± 0.2
	$D_{x,y}$[c]	21.0 ± 0.1	18.5 ± 0.1	19.4 ± 0.2
	A_{zz}[d]	0.99 ± 0.02	0.92 ± 0.02	0.96 ± 0.02
	$A_{x,y}$[d]	0.89 ± 0.01	0.78 ± 0.01	0.82 ± 0.01
Thr	D_{zz}[c]	8.01 ± 0.05	7.33 ± 0.05	7.70 ± 0.05
	$D_{x,y}$[c]	6.97 ± 0.05	5.99 ± 0.05	6.34 ± 0.05
	A_{zz}[d]	0.98 ± 0.01	0.90 ± 0.01	0.94 ± 0.01
	$A_{x,y}$[d]	0.86 ± 0.01	0.74 ± 0.01	0.78 ± 0.01
TMS	D_{zz}[c]	1.29 ± 0.03	1.24 ± 0.04	1.26 ± 0.03
	$D_{x,y}$[c]	0.62 ± 0.03	0.58 ± 0.03	0.61 ± 0.03

[a] Bicelle concentration in w/v, with q = [DMPC]/[DHPC] = 3.2. [b] Bicelles included CTAB in a molar ratio [DMPC]/[CTAB] = 20. [c] Self-diffusion coefficients in units of 10^{-10} m^2 s^{-1}. Errors in the self-diffusion coefficients are determined from the uncertainties in the fit. $D_{x,y}$ refers to the $(D_{xx} + D_{yy})/2$. [d] Obstruction factors ($A_{zz} = D_{zz}/D_0$; $A_{x,y} = D_{x,y}/D_0$) calculated using isotropic diffusion coefficients (D_0) of 23.6×10^{-10} m^2 s^{-1} for HDO and 8.15×10^{-10} m^2 s^{-1} for Thr, measured in the same buffer at 35 °C.

The conclusion that $D_{||} \approx 0$ for TMS is based on the initial rate of the transverse gradient decay curve and the assumption that $D_{zz} = D_{\perp}$. If the full transverse decay curve is sampled and fitted to eq 2c, a nonzero value for $D_{||}$ is found ($D_{||} \approx D_{\perp}/10$). If the domain size over which the bicelle bilayer normals remain parallel with one another were much smaller than the distance over which TMS diffuses (~10 μm) during the time of the experiment (600 ms), a monoexponential decay would have been observed (cf. eq 2d). If the domain size were much larger than 10 μm, a stronger nonexponentiality would be observed in fitting the decay data of Figure 1B, with $D_{||} \approx 0$. So, these data indicate that the domain size over which the bilayer normal remains correlated is on the order of 10 mm. For threonine and HDO, the difference between $D_{||}$ and $D_{\perp}$ is too small to permit observation of such nonexponential decay (see below).

Remarkably, the data presented in Table 2 indicate that the obstruction for threonine is consistently slightly stronger (lower A_{zz} and $A_{x,y}$) than for HDO. This is a counterintuitive result, since both are in the aqueous phase. A likely explanation for the stronger obstruction of threonine by the bicelles is a very weak attractive interaction between threonine and the bicelle surface. Other evidence, supporting such a very weak interaction is found in unusually large ^1JCH dipolar couplings, in the ±8 Hz range, which is much larger than predicted for such a small molecule on the basis of shape,[36] or compared to what is measured in the PEG medium. Therefore, for interpretation of the obstruction factors in terms of bicelle morphology, we will only focus on the HDO data.

For water, the transverse and longitudinal self-diffusion rates in bicelles are more similar to one another than for TMS, indicating that $D_{||}$ is nonzero. Assuming again that $D_{zz} = D_{\perp}$, and $D_{x,y} = (D_{||} + D_{\perp})/2$, $D_{||} = (15.3 \pm 0.3) \times 10^{-10}$ and $(16.1 \pm 0.3) \times 10^{-10}$ m^2 s^{-1} in the 10% bicelle solutions without and with CTAB, respectively, corresponding to $A_{||}$ values of 0.65 ± 0.02 and 0.68 ± 0.02. Although, as argued above on the basis of the TMS D_{zz} diffusion, the model of noninteracting disk shaped particles is an oversimplification for the liquid crystalline bicelle solution, it is interesting to see what disk diameter the transverse diffusion obstruction predicts in this standard model. There are no analytical expressions relating the obstruction factor to the diameter of a hemitoroidal bicelle (i.e.,

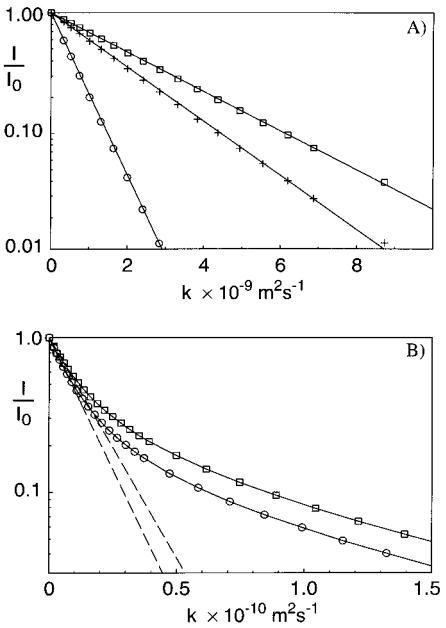

Figure 2. Tracer signal decay as a function of gradient strength in the (CP)Br liquid crystal, using a 600 ms diffusion delay. (A) Signal decay for HDO (O), threonine (+), and TMS (□) when using z gradients. (B) HDO signal decay as a function of gradient strength in the *x* direction (□) and in the *y* direction (O). The dashed lines correspond to the initial decay rates; solid lines are shown to guide the eye.

a disk with its rim covered by the outer half of a toroid[25,71]). However, at large aspect ratios, $A_{||}$ for a hemitoroidal disk will be very similar to that of an oblate spheroid of the same aspect ratio. At large aspect ratios, the volume of an oblate spheroid of diameter, $2R_L$, and thickness $2R_S$, is smaller by a factor $4R_L^2/[6(R_L - R_S)^2 + 3\pi R_L R_S]$ than a hemitoroidal disk of diameter $2R_L$ and thickness $2R_S$. Lowering the oblate spheroid volume fraction, Φ, by this factor relative to the 9.6% (v/v) fraction of bicelles, eq 5a yields aspect ratios of 9.7 ± 0.7 and 8.8 ± 0.6 for the bicelles in the absence and presence of CTAB. Assuming a bilayer thickness of 40 Å, this corresponds to a bicelle diameter of 390 ± 30 Å for 10% w(/v) sample in the absence of CTAB and a slightly smaller value of 350 ± 25 Å in the presence of CTAB. Note, however, that this diameter is nearly 3-fold smaller than the minimum size needed for nematic liquid crystalline ordering of rigid disks of 40 Å thickness at 9.6% (v/v).[75]

Cetylpyridinium Bromide Liquid Crystal. The second medium for which we report diffusion anisotropy data concerns a mixture of cetylpyridinium bromide, *n*-hexanol and NaBr in water.[29] At 25 °C, after overnight equilibration in a 600 MHz magnet, a solvent ^{2}H quadrupole splitting of 17.5 Hz was observed, in good agreement with the previously reported value of 17.9 Hz,[29] confirming the formation of a liquid crystalline phase.

Tracer signal decay resulting from diffusion in the *z* direction was again perfectly exponential (Figure 2A), and diffusion rates and obstruction factors are listed in Table 3. Considering that the volume fraction of the CPBr is smaller than that of the bicelle sample, the stronger obstruction for diffusion in the *z* direction ($A_{zz} \approx 0.85$ for CPBr and $A_{zz} \approx 0.95$ for bicelles) is perhaps surprising. Obstruction in the *z* direction may either result from the presence of defects, such as bridges between bilayers, or from imperfect alignment of the bilayers. However, considering that the transverse diffusion is indicative of a perfect lamellar phase with $D_{||} = 0$ (see below), we believe imperfect alignment

(75) Veerman, J. A. C.; Frenkel, D. *Phys. Rev. A* **1992**, *45*, 5632−5648.

Table 3. Self-Diffusion Coefficients and Obstruction Factors of HDO, Thr, and TMS in CPBr Liquid Crystal Solution at 25 °C[a]

	HDO	Thr	TMS
D_{zz}[b]	15.8 ± 0.2	5.2 ± 0.1	3.78 ± 0.1
$D_{x,y}$[b]	7.7 ± 0.2	2.5 ± 0.1	1.84 ± 0.1
A_{zz}[c]	0.85 ± 0.02	0.82 ± 0.01	
$A_{x,y}$[c]	0.41 ± 0.02	0.39 ± 0.02	

[a] For a 6% (w/v) CPBr liquid crystal, measured using a 600 ms diffusion interval. [b] Self-diffusion coefficients in units of 10^{-10} m^2 s^{-1}. Errors in the self-diffusion coefficients are determined from the uncertainties in the fit. $D_{x,y}$ refers to the $(D_{xx} + D_{yy})/2$. [c] Obstruction factors ($A_{zz} = D_{zz}/D_0$; $A_{x,y} = D_{x,y}/D_0$) calculated using isotropic diffusion coefficients (D_0) of 18.6×10^{-10} m^2 s^{-1} for HDO and 6.33×10^{-10} m^2 s^{-1} for threonine, measured in the same buffer at 25 °C.

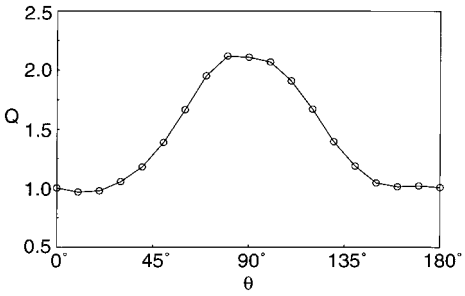

Figure 3. Transverse diffusion of TMS in CPBr liquid crystal. Plotted is the signal attenuation ratio, $Q = I(g(\theta))/I(g_x)$, for a fixed gradient strength of 25 G/cm, as a function of the angle θ between the gradient and the *x* axis (after first rotating the sample such that diffusion is slowest in the *x* direction).

or long-range undulations to be the dominant cause of the obstruction. Alignment of the CPBr liquid crystal relative to the magnetic field is a very slow process, and it is likely that even after the overnight equilibration used in the present experiments alignment remains imperfect. If the bilayer normal orientation is static and, on average, deviates from the transverse plane by an angle of 25°, this reduces D_{zz} by $\cos^2(25°)$, i.e. by 15%.

For signal decay resulting from self-diffusion in the transverse direction, an unexpected dependence of the decay rate on the direction of the transverse gradient is found. Figure 2B shows the HDO signal decay as a function of gradient strength in the *x* and *y* directions, with the sample aligned relative to the gradients such that the *x* gradient yields the slowest diffusion rate. Analogously, Figure 3 plots the TMS signal attenuation $Q = I(g = 1.25$ G/cm$)/I(g = 25$ G/cm) as a function of the direction in which the gradient is applied. The dependence of *Q* on the gradient direction has the same shape and nearly the same amplitude for all three tracers (data not shown), indicating that their relative decay rates have the same dependence on gradient orientation.

The dependence of the diffusion rate on the direction of the transverse gradient indicates that the bilayer normal orientation remains correlated in the *xy* plane for a significant fraction of the NMR sample. Diffusion in the direction that is, on average, most orthogonal to the bilayer planes is slowest and highly nonexponential. The initial rate of the corresponding decay curve (Figure 2B) corresponds to the sample volume fraction that has bilayer planes mostly parallel to the gradient direction, whereas the majority of the signal decays much more slowly, at rates that depend on the angle between the bilayer normal and the gradient direction (cf. eqs 2a,c). For a gradient direction that is, on average, more parallel to the bilayer planes, the opposite is observed, with a larger fraction of the signal decaying rapidly and a smaller fraction exhibiting much slower decay. The

Table 4. Self-Diffusion Coefficients and Obstruction Factors of HDO, Thr, and TMS in $C_{12}E_5$ Liquid Crystal at 25 °C[a]

	HDO	Thr	TMS
D_{zz}[b]	14.7 ± 0.1	4.9 ± 0.1	2.2 ± 0.1
$D_{x,y}$[b]	7.2 ± 0.3	2.4 ± 0.1	1.05 ± 0.05
A_{zz}[c]	0.79 ± 0.01	0.77 ± 0.01	
$A_{x,y}$[c]	0.39 ± 0.02	0.38 ± 0.02	

[a] For a 8% (w/w) $C_{12}E_5$ liquid crystal, measured using a 600 ms diffusion interval. [b] Self-diffusion coefficients in units of 10^{-10} m^2 s^{-1}. Errors in the self-diffusion coefficients are determined from the uncertainties in the fit. $D_{x,y}$ refers to the $(D_{xx} + D_{yy})/2$. [c] Obstruction factors ($A_{zz} = D_{zz}/D_0$; $A_{x,y} = D_{x,y}/D_0$) calculated using isotropic diffusion coefficients (D_0) of 18.6 × 10^{-10} m^2 s^{-1} for HDO and 6.33 × 10^{-10} m^2 s^{-1} for threonine.

transverse diffusion rates reported in Table 3 correspond to $[(D_{xx}^2 + D_{yy}^2)/2]^{1/2}$, as measured from the initial slopes of the nonexponential decays.

$C_{12}E_5$-Based Liquid Crystal. For the $C_{12}E_5$-based liquid crystal, a lamellar phase with a superstructure in which the bilayers bend into sets of concentric cylinders has been proposed, similar to structures observed in freeze−fracture transmission electron micrographs of ternary tetradecyldimethylaminoxyde/*n*-heptanol/water mixtures.[37] These cylinders are believed to align with their common axis parallel to the magnetic field.[31,60] Although diffusion in the *z* direction in such a concentric cylinder α-lamellar phase is indistinguishable from that in a planar lamellar phase, transverse diffusion is predicted to be different. This difference becomes more pronounced when the diameter of the most outer cylinder is smaller than the distance over which a tracer molecule can diffuse during the NMR experiment. A model for NMR signal decay resulting from transverse diffusion of a tracer molecule, confined between concentric cylinders, is presented in the Appendix. To test the validity of this proposed morphology, the self-diffusion data obtained in the $C_{12}E_5$ liquid crystal are fitted to the concentric cylinder diffusion model described in the Appendix and also to the regular model for diffusion in an ordered lamellar phase (eq 2c).

The experimental self-diffusion data in the *z* direction for the three tracer molecules present in the $C_{12}E_5$ liquid crystal are all monoexponential (Supporting Information Figure 2), and the derived rates are summarized in Table 4. Diffusion obstruction in the *z* direction is significant and even slightly stronger than in the CPBr medium. This indicates the presence of rather substantial deviations from 90° between the bilayer normal and the magnetic field direction, or the presence of obstructions, or both. These obstructions could be visualized as either "caps" on the concentric cylinders, "bridges" between adjacent bilayers (Figure 4B) or small globular structures such as micelles or vesicles present in the system. In the phase diagram of $C_{12}E_5$, the NMR conditions are very close to where the system switches from the α-lamellar phase, L_α, to a mixed $L_\alpha + L_3$ phase, a state (referred to as a "sponge" phase) that is closely related to the L_α phase, and the partial presence of which cannot be fully excluded.[62]

As was the case for the CPBr liquid crystal, the transverse self-diffusion of none of the three tracer molecules in the $C_{12}E_5$-based liquid crystal is monoexponential (Supporting Information Figure 3). Figure 5 compares the various models for self-diffusion of threonine in the *x* direction. The curves in Figure 5 represent fits of various models to the first 40% of the decay curve, such as to emphasize the discrepancy between the models and the experimental data. For both the α-lamellar and the concentric cylinder models, the value for $D_\perp = D_{zz}$ is taken from the fit to the monoexponential decay observed in the *z* direction (Table 4). The optimal fit to the lamellar model requires a nonzero value of $D_\parallel$ ($D_\parallel = 6.54 \times 10^{-12}$ m^2 s^{-1}, $D_\perp/D_\parallel = 75$), indicating that threonine can traverse the $C_{12}E_5$ bilayer, albeit at a very slow rate.

When comparing the threonine transverse diffusion decay data to those predicted for a medium of oriented concentric cylinders (see Appendix), the value for $D_\parallel$ is assumed to be zero. So the diffusion rate itself is not optimized and simply taken from D_{zz}, but the radius of the outer cylinder, R_{max}, affects the shape of the transverse decay curve. Clearly, for very large values of R_{max} the concentric cylinder model becomes indistinguishable from the planar lamellar model with $D_\parallel = 0$. For values of R_{max} that are small relative to the distance over which the molecule can diffuse in the 600 ms between pulsed field gradients, the decay at stronger gradients will be strongly inhibited. The dotted line in Figure 5 corresponds to the predicted decay curve for a

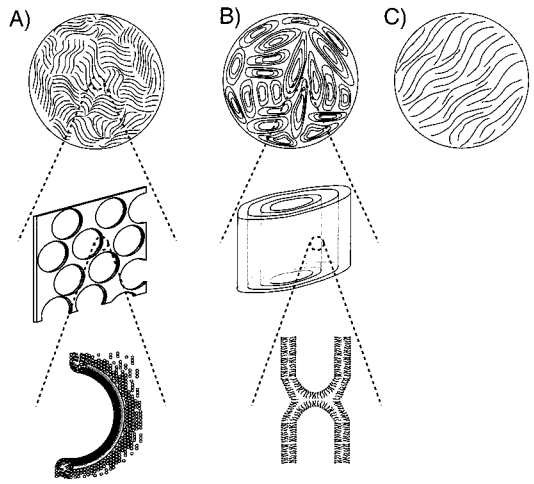

Figure 4. Schematic morphology representation for the three different types of lamellar liquid crystalline media studied, as determined by tracer diffusion anisotropy: (A) ordered bicelles; (B) PEG/*n*-hexanol; (C) CPBr. The top views in A−C depict slices orthogonal to the NMR sample tube, which has its axis parallel to the magnetic field. Lower panels illustrate (A) the pores in the DMPC bilayer with the rims covered by detergent and (B) a bridge-type structure between bilayers in the PEG/*n*-hexanol medium, inferred from relatively high HDO diffusion obstruction in the *z* direction and nonzero TMS diffusion in the direction parallel to the bilayer normal. The flattened concentric cylinder model for PEG/*n*-hexanol is compatible with the NMR diffusion data, but cannot be distinguished from a planar lamellar phase, such as shown in the top panel of A.

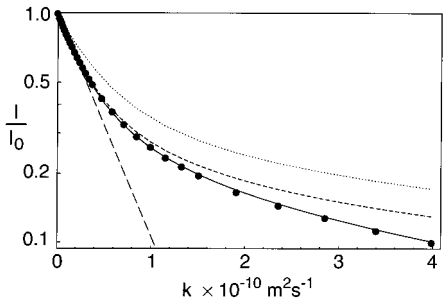

Figure 5. The threonine signal intensity decay as a function of transverse gradient strength in liquid crystalline $C_{12}E_5$/hexanol medium at 25 °C. Long dashes correspond to an exponential fit to the initial slope of the decay curve. Short dashes correspond to the lamellar model (eq 2c) with $D_\perp = D_{zz} = 4.88 \times 10^{-10}$ m^2 s^{-1} and $D_\parallel = 0$; the solid line corresponds to the lamellar model with $D_\perp = 4.88 \times 10^{-10}$ m^2 s^{-1} and $D_\parallel = 6.5 \times 10^{-12}$ m^2 s^{-1}; the dotted line is the cylindrical model with $D_\perp = 4.88 \times 10^{-10}$ m^2 s^{-1} and $D_\parallel = 0$, for $R_{min} = 1$ μm and $R_{max} = 40$ μm.

R_{max} value of 40 μm, and even at this relatively large value the planar lamellar model (short dashes for $D_{||} = 0$, solid line for $D_{||} \neq 0$) fits the diffusion decay data better than the concentric cylinder model. These data do neither exclude nor confirm a superstructure of concentric cylinders, made up of lamellar $C_{12}E_5$ bilayers. However, if the superstructure of concentric cylinders indeed applies, the minimum value for R_{max} is on the order of 50 μm. At $R_{max} \gg 50$ μm the planar lamellar and concentric cylinder lamellar models become indistinguishable by PFG NMR; at $R_{max} < 50$ μm the fit to the experimental data, including the initial slope, becomes progressively worse.

For HDO diffusion, the best fit is also obtained for the planar lamellar model, with $D_{\perp} = D_{zz} = 14.7 \times 10^{-10}$ m^2 s^{-1} (again obtained from independent measurement of D_{zz}) and $D_{||} = 0.88 \times 10^{-10}$ m^2 s^{-1} ($D_{\perp}/D_{||} = 17$). Fits to the concentric cylinder model and the planar lamellar model are compared in Supporting Information Figure 3. The permeability of the $C_{12}E_5$ bilayers to water, as evidenced by the smaller value of $D_{\perp}/D_{||}$, appears somewhat higher than for threonine.

The transverse TMS diffusion data also exclude monoexponential decay and fit much better to the nonexponential decay curves predicted by the planar lamellar and concentric cylinder lamellar models (Supporting Information Figure 4). For the planar lamellar model we find $D_{||} = 0.037 \times 10^{-10}$ m^2 s^{-1}, with $D_{\perp}$ again obtained from the D_{zz} measurement ($D_{zz} = 2.24 \times 10^{-10}$ m^2 s^{-1}; $D_{\perp}/D_{||} = 60$). The nonzero value of $D_{||}$ indicates that TMS can diffuse, albeit at a very slow rate, in the direction parallel to the bilayer normal.

Concluding Remarks

Measurement of tracer self-diffusion rates, and in particular their diffusion anisotropy, is a very informative tool for studying the morphology of dilute liquid crystalline media.[39−45] The tracer diffusion data reported here are consistent with a disklike morphology of the bicelles below the DMPC melting temperature (25 °C). This agrees with conclusions from a very recent small-angle neutron scattering study on Tm^{3+}-doped bicelles.[76] The obstruction and self-diffusion data indicate disk radii in the 250 Å range. Above the DMPC melting temperature the solution becomes liquid crystalline. When the HOD transverse obstruction factor in this liquid crystalline medium is interpreted in terms of the common, inert bicellar disk suspension, a diameter in the 350−400 Å range is obtained, in good agreement with earlier model calculations.[25] However, diffusion of the lipid-soluble TMS in the direction of the magnetic field shows a rapid increase above the DMPC melting temperature and a diffusion rate that is much faster than compatible with a 400 Å diameter bicelle. This indicates that TMS can rapidly exchange between bicelles, which therefore must make (transient) contacts in an edge-on manner. This paints a different picture of the liquid crystal bicelle suspension and may explain the so far puzzling observation that bicelle suspensions can retain a stable nematic liquid crystalline order down to as low as 2%, i.e., at concentrations that are more than an order of magnitude lower than the Onsager limit for liquid crystal formation of neutral 400 Å diameter disks. The Onsager theory predicts that liquid crystalline ordering of flat, infinitely thin disks of radius R requires $B_2c_p > 4.2$, where the second virial coefficient B_2 describes the effective volume ($\pi^2R^3/2$) and c_p the particle concentration.[78] Monte Carlo calculations for disks with an aspect ratio of 10, as applies for the idealized bicelle, only marginally change this condition to $B_2c_p > 3.9$.[75]

The picture emerging from the TMS and HOD diffusion data is intermediate between a regular a-lamellar phase and the common discotic nematic suspension. Edge-to-edge interactions between the disks make it equivalent to a strongly perforated bilayer, in which the bilayer rims surrounding the holes consist of DHPC (Figure 4A). This picture of a highly dynamic, perforated bilayer is consistent with the tracer diffusion data reported here and resolves the question of why the bicelle solution remains liquid crystalline at such low volume fractions. Sanders and Prosser have also questioned the inert-bicelle model and reported that polarizing microscope data indicate that the bicelles may be interconnected.[26] A very recent small-angle neutron scattering study on Tm^{3+}-doped bicelles, oriented with their normal parallel to the magnetic field,[77] provides independent support for a perforated lamellar phase morphology.[76] Below the DMPC melting temperature our diffusion data indicate the bicelle particles to be disk-shaped, but their limited aspect ratio (ca. 6) prohibits liquid crystalline ordering and explains the absence of such order below 25 °C. Another very recent small-angle neutron scattering study indicates that at [DHPC]/[DMPC] ratios much higher than those used in our study, where no liquid crystalline bicelle ordering occurs, the disk-shaped morphology applies both below and above the DMPC melting temperature.[51]

In the liquid crystalline bicelle phase, the transverse TMS diffusion decay is strongly nonexponential. This indicates that the orientations of bilayer normals remain strongly correlated over the distance that TMS diffuses between the encoding and decoding pulsed field gradients and thereby puts a minimum size limit of ca. 10 μm on the domain size (Figure 4A). TMS diffusion in the z direction is nearly independent of the bicelle concentration (Table 2), even at much higher concentrations than shown. This indicates that the perforated bilayer morphology applies to the entire region of the phase diagram where the sample adopts liquid crystalline order.

The CPBr diffusion anisotropy data under the conditions used for studying biological macromolecules are only compatible with a lamellar phase, and exclude the possibility of wormlike morphologies. The observation that $D_{||} = 0$ for all three tracer molecules indicates the virtual absence of holes in the bilayers or bridges between them and suggests a picture of a very regular, nearly defect free α-lamellar phase. The surprising finding that the transverse diffusion rates are a function of the direction of the transverse gradient relative to the sample indicates that the distribution of the bilayer normals in the transverse plane is not random (Figure 4C), and points to a large persistence length for the lamellar plane orientations, on the order of millimeters.

Tracer diffusion anisotropy of the $C_{12}E_5$/hexanol/water medium confirms it to be a lamellar phase. However, nonzero diffusion rates in the direction orthogonal to the bilayers for all three tracer molecules suggests the presence of a small fraction of defects, i.e., holes in the bilayers and bridges between bilayers. Considering the proximity of the sample preparation studied to the L_3 or sponge phase in the phase diagram of this mixture,[61,62] this is perhaps not surprising. The presence of a superstructure of concentric cylinders could neither be confirmed nor disproven on the basis of the tracer diffusion data. For the case where the outer cylinder diameter of such a set of concentric cylinders is much larger than the distance over which the tracer molecules diffuse in the transverse direction between encoding and decoding gradients, the simple lamellar model and the concentric cylinder models predict identical results.

(76) Nieh, M. P.; Glinka, C. J.; Krueger, S.; Prosser, R. S.; Katsaras, J. *Langmuir* **2001**, *17*, 2629−2638.
(77) Prosser, R. S.; Hunt, S. A.; DiNatale, J. A.; Vold, R. R. *J. Am. Chem. Soc.* **1996**, *118*, 269−270.
(78) Onsager, L. *Ann. N. Y. Acad. Sci.* **1949**, *51*, 627−659.

However, if the concentric cylinder morphology indeed is present, the diffusion data indicate a minimum diameter of ca. 50 μm for the outer shell of such a set of concentric cylinders. The absence of heterogeneity in the observed ^{2}H splitting indicates the absence of voids between adjacent sets of cylinders, and therefore requires significant distortion from the ideal cylinder model, and a situation where the cylinders are significantly flattened in order to reduce void formation (Figure 4B). The $C_{12}E_5$/hexanol/water mixture presents a very convenient and robust liquid crystalline medium that has low surface charge density and therefore causes solute alignment primarily through a steric mechanism.

Acknowledgment. We thank Markus Zweckstetter for help with the data analysis and preliminary experiments on the CPBr medium and Jerome Boisbouvier for careful reading of the manuscript. This work was supported by the AIDS Targeted Anti-Viral Program of the Office of the Director of the National Institutes of Health. S.G. acknowledges financial support from The Netherlands Organization for Scientific Research (NWO).

Appendix: Gradient Echo Decay for Diffusion in a Set of Concentric Cylinders

The probability distribution for a particle exhibiting uninhibited diffusion in one dimension is given by

$$P(x) = (4\pi D\Delta)^{-1/2} e^{-(x-x_0)^2/4D\Delta} \quad \text{(A.1)}$$

where $x - x_0$ describes the net displacement of a particle starting at position x_0 and diffusing to x with a self-diffusion coefficient D during a time interval Δ. For diffusion on the surface of a cylinder with diameter $2R$ and its axis parallel to the z axis of the static magnetic field, eq A.1 transforms into

$$P(\theta) = Ae^{(-R^2(\theta-\theta_0)^2)/4D\Delta} \quad \text{(A.2)}$$

where A is a normalization constant and θ_0 and θ are the starting and final angles relative to the x-axis in which the gradient is being applied.

The degree of dephasing caused by the applied gradients is proportional to the displacement in the direction of the applied pulsed field gradients. In the short gradient pulse limit, the dephasing of the signal of a nucleus displaced by $x - x_0$ in the direction of the pulsed field gradient (of magnitude g and duration δ) is given by

$$\phi = \gamma g \delta (x - x_0) \quad \text{(A.3)}$$

where γ is the gyromagnetic ratio of the nuclear spin observed. With $x = R \cos \theta$ and $x_0 = R \cos \theta_0$, the echo signal after diffusion during the delay Δ, which separates the encoding and decoding gradients, may be written as

$$S(\Delta) = 2\pi \mathrm{R} \int_{\theta_0=0}^{2\pi} \int_{\theta=-\infty}^{+\infty} P(\theta) \cos(\phi)\, \mathrm{d}\theta\, \mathrm{d}\theta_0 \quad \text{(A.4)}$$

where ϕ is the degree of dephasing (eq A.3) and $P(\theta)$ the probability distribution of eq A.2. The prefactor $2\pi R$ reflects the scaling of the number of particles as a function of cylinder diameter. For a set of closely spaced concentric cylinders, with radii ranging from R_0 to R_{max}, the total signal intensity is given by

$$S(\Delta) = \int_{R_0}^{R_{max}} 2\pi R \int_{\theta_0=0}^{2\pi} \int_{\theta=-\infty}^{+\infty} P(\theta) \cos(\phi)\, \mathrm{d}\theta\, \mathrm{d}\theta_0\, \mathrm{d}R \quad \text{(A.5)}$$

Supporting Information Available: Figures showing the exponential tracer diffusion decay data for isotropic bicelles at 20 °C and in the z dimension for the $C_{12}E_5$ medium, HDO transverse diffusion decay in $C_{12}E_5$, and TMS transverse diffusion decay in $C_{12}E_5$ and tables detailing diffusion rates derived from experiments with a 150 ms diffusion delay (PDF). This material is available free of charge via the Internet at http://pubs.acs.org.

JA011967L